

Toward more accurate estimates of carbon emissions from small reservoirs

Laura C. Naslund ,^{1*} Andrew S. Mehring ,² Amy D. Rosemond ,¹ Seth J. Wenger ¹

¹Odum School of Ecology, University of Georgia, Athens, Georgia, USA

²Department of Biology, University of Louisville, Louisville, Kentucky, USA

Abstract

Because of their abundance and high emissions rates, small reservoirs (< 0.01 km²) can be important emitters of the greenhouse gases carbon dioxide and methane. However, emissions estimates from small reservoirs have lagged those of larger ones, and efforts to characterize small reservoir emissions have largely overlooked variations in emissions pathways, times, and locations. We intensively sampled four small reservoirs in Georgia, USA, during the summer to quantify the contribution and spatiotemporal variability of different emissions pathways (CO₂ and CH₄ diffusion, CH₄ ebullition). We used these data to evaluate the efficiency and accuracy of different sampling schemes. Every emissions pathway was dominant in one reservoir on one sampling day, and excluding ebullition caused misestimation between –89% and –15% of the total flux. Sampling only once daily caused misestimation between –78% and 45%, but sampling twice or just after dawn (07:00 h) reduced error. Sampling four or fewer locations caused misestimation between –85% and 366%, and our results indicated that 6–20 sampling locations may be needed for reasonable accuracy. The floating aquatic macrophyte *Wolffia* sp. (duckweed) appeared to exert control over emissions variability, and the consequences of not accounting for variability were greater in a duckweed-covered reservoir. Our results indicate that sampling only at 10:00 h (modal sampling time of prior efforts) may lead to the erroneous conclusion that reservoirs with high photosynthetic biomass are CO₂ sinks rather than sources. Improving estimation accuracy by accounting for within-reservoir variation in emissions will facilitate more strategic management of these abundant, anthropogenic ecosystems.

Of the millions of reservoirs that exist globally, most have surface areas < 0.01 km² (Downing 2010). As a consequence of their numeric abundance and positions in river networks as recipients of substantial terrestrially derived carbon inputs (Harvey and Schmadel 2021), these reservoirs have the capacity to cumulatively emit carbon dioxide (CO₂) and methane (CH₄) in comparable magnitudes to larger reservoirs (Grinham

et al. 2018; Ollivier et al. 2019a), which have been the primary focus of research for the past two decades. Variation in the dominant pathways, times, and locations of emissions in natural lakes and larger reservoirs has been shown to impact inferences about the total magnitude of their emissions (Beaulieu et al. 2016; Sieczko et al. 2020; Hounshell et al. 2023); however, this variation has been poorly characterized in small reservoirs, and prior efforts to estimate their emissions have frequently relied on measurements of one pathway of emissions, at one time during the day, and in few locations in the reservoir (Wang et al. 2017; Webb et al. 2019; Ollivier et al. 2019a). Unaccounted-for variation in emissions may lead to misestimation of the contribution of small reservoirs to landscape greenhouse gas (GHG) emissions, which may be reduced or mitigated through management actions.

Reservoirs can yield high CO₂ and CH₄ emissions by concentrating substantial volumes of organic matter from both terrestrial sources and in situ primary production, leading to high rates of decomposition and respiration, depletion of dissolved oxygen (DO), and facilitation of anaerobic metabolic pathways, including methanogenesis (Friedl and Wüest 2002). The resulting CO₂ and CH₄ can be emitted from reservoirs by

*Correspondence: laura.naslund@uga.edu

This is an open access article under the terms of the [Creative Commons Attribution-NonCommercial](https://creativecommons.org/licenses/by-nc/4.0/) License, which permits use, distribution and reproduction in any medium, provided the original work is properly cited and is not used for commercial purposes.

Additional Supporting Information may be found in the online version of this article.

Author Contribution Statement: L.C.N.: Conceptualization (equal); investigation (lead); writing – original draft (lead); formal analysis (lead); writing – review and editing (equal). A.S.M.: Conceptualization (equal); writing – reviewing and editing (equal); resources (equal); formal analysis (supporting); methodology (equal); supervision (equal). A.D.R.: Conceptualization (equal); writing – review and editing (equal); resources (equal); supervision (equal). S.J.W.: Conceptualization (equal); formal analysis (supporting); supervision (equal); writing – review and editing (equal).

the diffusion of gas from high to low concentration across the water–air interface (Deemer et al. 2016). CH₄ can also be emitted by bubbles that rise through the water column from the sediment in a process known as ebullition.

These bubbles form when the partial pressure of the accumulated gas surpasses the pressure on the sediments and overcomes water surface tension (Harrison et al. 2017). Ebullition can contribute substantially to radiative forcing from reservoirs because much of the CH₄ transported in bubbles can escape oxidation in the water column (Bastviken et al. 2008), and one molecule of CH₄ has the same warming potential as 27 molecules of CO₂ (Forster et al. 2021). A global synthesis of GHG emissions from mostly larger reservoirs found that ebullition contributed on average 65% of total CH₄ flux (Deemer et al. 2016), yet ebullition has not been included in many past efforts to characterize emissions from small reservoirs (Wang et al. 2017; Ollivier et al. 2019a; Peacock et al. 2019; Webb et al. 2019). If ebullition is a dominant pathway of CO₂-equivalent (CO₂-eq) emissions from small reservoirs, sampling efforts that fail to include it will underestimate total emissions.

Ebullition can exhibit spatial variation associated with depth and distance from the reservoir inlet, which may also impact total emissions estimates (Natchimuthu et al. 2016; Linkhorst et al. 2021). At shallower depths, CH₄ bubbles can grow and escape the sediment more easily because there is lower hydrostatic pressure to overcome (Boudreau 2012). There is also a diminished opportunity for CH₄ to be oxidized during the transport of bubbles through the shorter water column to the water surface (Bastviken et al. 2008). At the reservoir inlet, ebullition can be higher due to greater accumulation of watershed-derived carbon as particles in transport settle (Natchimuthu et al. 2016). This greater organic carbon availability can result in higher CH₄ production near the reservoir inlet (Maeck et al. 2013). The influence of depth and inlet distance on rates of CH₄ ebullition can create longitudinal patterns of declining ebullition from the inlet to the dam, which has been observed in larger reservoirs (Beaulieu et al. 2016; McClure et al. 2020; Linkhorst et al. 2021). Patterns of CH₄ and CO₂ diffusion have also been observed in larger reservoirs arising from spatial heterogeneity in gas production and in rates of gas transfer (Paranaíba et al. 2018). If small reservoirs exhibit substantial spatial heterogeneity in emissions, failing to account for this variability may lead to misestimation of emissions.

CO₂ and CH₄ diffusion, like many biogeochemical processes, may exhibit daily temporal patterns due to the overriding influence of the sun on the light, wind, pressure, and temperature conditions that can influence the magnitude of emissions (Nimick et al. 2011; Natchimuthu et al. 2014; Siczko et al. 2020). If small reservoirs exhibit diel patterns of diffusion, these patterns may be important to incorporate into the estimation of daily emissions from discrete measurements in time. Diffusion is a product of both the supply and transfer of gases to the atmosphere, and both factors have drivers that can exhibit diel patterns, potentially yielding diel fluctuations

in emissions (Cole and Caraco 1998). First, CO₂ supply can be altered by photosynthetic activity. When light is available for photosynthesis, autotrophs can take up CO₂, reducing its supply, yielding lower daytime CO₂ emissions (Natchimuthu et al. 2014; Gómez-Gener et al. 2021). Autotrophic activity may also reduce daytime diffusive CH₄ emissions by increasing surface DO concentrations, promoting higher rates of CH₄ oxidation and lower CH₄ supply (Ford et al. 2002).

When transfer rather than supply processes dominate, however, the pattern of lower daytime CO₂ and CH₄ diffusion may be reversed. Wind is a major driver of surface turbulence and gas exchange in reservoirs (Crusius and Wanninkhof 2003). Windspeeds are generally higher during the day, which can force higher rates of gas exchange and, thus, higher daytime diffusive emissions (Siczko et al. 2020; Hounshell et al. 2023). Transfer processes can also impact patterns of CH₄ ebullition, with drops in hydrostatic pressure yielding high bubbling rates; however, few studies have captured sub-daily measurements of CH₄ emissions to characterize the periodicity of bubbling events (but see Grinham et al. 2011; Varadharajan and Hemond 2012; Siczko et al. 2020). If either supply or transfer processes generate diel contrasts in CO₂ and CH₄ emissions, failing to account for these temporal patterns—for example, by only sampling during daytime hours—may also lead to misestimation of total emissions.

To support accurate estimation of small reservoir GHG emissions, we quantified (1) the contribution of different pathways of emissions, (2) temporal variation in emissions, and (3) spatial variation in emissions from four small reservoirs during the summer in the southeastern U.S. Specifically, we measured CH₄ and CO₂ diffusion at 12 sampling stations and CH₄ ebullition at 25 sampling stations every 3 h over at least one 24-h cycle in each of the small reservoirs. We used data from this intensive sampling to simulate the consequences of different sampling schemes to identify those that efficiently yielded accurate estimates of total daily emissions.

Materials and methods

We sampled four small reservoirs within a 3 km² area in Athens, GA, USA, in August–September 2022 (Supporting Information Fig. S1). August and September are among the hottest months of the year, and studies in similar climatic zones have found that they contribute large proportions of total annual emissions (van Bergen et al. 2019; McClure et al. 2020). The reservoirs ranged in area from 0.0012 to 0.0077 km² and in mean depth from 0.80 to 2.03 m (Table 1). We estimated their water residence time to be 19–46 d based on discharge estimates from a regional regression equation with average annual precipitation and watershed area (Gotvald 2017). At the time of sampling, a floating macrophyte in the genus *Wolffia*, an angiosperm in the family Lemnaceae hereon referred to as duckweed, extensively covered the surface of one reservoir

Table 1. Reservoir sampling dates, physical, and chemical characteristics. All sites were sampled in 2022. Temperature, dissolved oxygen, and pH values reported here are spot measurements taken at four locations in each reservoir during every diffusive sampling flux period. We also recorded dissolved oxygen using a continuous sensor at the top of the water column in the deepest location in the reservoir (Supporting Information Fig. S4).

Site name	Area (km ²)	Max depth (m)	Mean depth (m)	Residence time (d)	Dates sampled	Temperature (°C)	Dissolved oxygen (mg L ⁻¹)	pH
Sister	0.0012	2.27	1.25	20	22–23 Aug	Top: 27.4±0.6 Bottom: 26.7±0.4	Top: 7.0±0.5 Bottom: 5.5±1.4	Top: 8.0±0.4 Bottom: 7.6±0.4
Catfish	0.0018	1.98	0.80	19	06–07 Sep	Top: 26.0±0.6 Bottom: 25.5±0.3	Top: 4.6±0.4 Bottom: 4.0±1.2	Top: 7.2±0.1 Bottom: 7.2±0.1
					18–19 Sep	Top: 22.0±0.6 Bottom: 21.6±0.3	Top: 5.4±0.6 Bottom: 4.8±1.2	Top: 7.2±0.1 Bottom: 7.2±0.1
Deans	0.0042	3.52	2.03	46	16–17 Aug	Top: 28.6±0.6 Bottom: 28.0±0.4	Top: 6.2±0.5 Bottom: 4.4±2.1	Not available
					30–31 Aug	Top: 28.6±0.9 Bottom: 27.6±0.6	Top: 6.0±0.6 Bottom: 3.4±2.5	Top: 7.5±0.1 Bottom: 7.2±0.3
Blue Herron	0.0077	3.8	1.58	45	13–14 Sep (duckweed coverage: 100%)	Top: 24.4±1.1 Bottom: 23.2±1.1	Top: 0.7±0.8 Bottom: 0.3±0.4	Top: 6.9±0.3 Bottom: 6.8±0.2

(Blue Herron). The other three sites had minimal or no macrophyte coverage and no visual evidence of a phytoplankton bloom (Supporting Information Fig. S1). Although not an initial objective of our study, we took this opportunity to evaluate the potential role of duckweed on the magnitude and spatio-temporal patterns of emissions in addition to the objectives outlined above. Every 3 h, we measured CO₂ and CH₄ diffusion at 12 locations and CH₄ ebullition at 25 locations for one to two 24-h cycles in each reservoir to evaluate patterns in the pathways, times, and locations of emissions (Table 1). Because we observed a high CH₄ concentration at the surface of Blue Herron near the intake for the reservoir outlet, we additionally calculated the flux of CH₄ from degassing as water is discharged over the reservoir outlet, which can be a major pathway of CO₂-eq emissions in larger reservoirs (Kemenes et al. 2007; Maeck et al. 2013).

Measuring emissions pathways

We measured ebullition in each reservoir every 3 h over 24-h periods at 25 sampling stations (Supporting Information Fig. S2a). The sampling stations were positioned at different distances from the reservoir perimeter and divided among five transects, which we installed using rope fixed diagonally across the width of the reservoir to capture variation in sampling station depth and distance to the inlet. At each sampling station, we installed an ebullition trap by affixing it to the rope with a zip tie. This method of trap installation permitted us to sample ebullition without disturbing the sediment. The

ebullition traps consisted of inverted funnels with 18 cm diameters fastened to 60 mL polypropylene syringes with silicone sealant. At the start of the sampling, we filled the traps with water by evacuating air through a three-way stopcock, fastened polyethylene foam to the syringe for buoyancy, and weighted the funnel so that only the syringe was above the water. As bubbles rose from the sediment, they displaced the water and collected at the top of the syringe where we emptied the gas through the stopcock.

Every 3 h we recorded the volume of gas accumulated in the ebullition trap syringe. If the volume exceeded 18 mL, we emptied the trap and injected the contents into a pre-evacuated 12-mL glass vial with a chlorobutyl and PTFE/silicon septum. At the end of the 24-h period, we emptied all traps, combining gas from traps as necessary to obtain 18 mL. After all other measurements had been taken, we physically disturbed the sediment in three locations along the edges of the reservoir to collect fresh bubbles. We compared concentrations of the fresh bubbles to those that had been left in the ebullition traps during the sampling period to evaluate whether the oxidation of CH₄ bubbles in the traps impacted the concentrations of the collected gas. On return to the lab, we analyzed the CH₄ concentrations of the collected gas using an SRI Instruments 8610C Gas Chromatograph equipped with a methanizer and Flame Ionization Detector (GC-FID). We did not find a significant difference between the concentrations of gas collected in the traps and fresh bubbles, so we used concentrations from both collection methods to estimate total ebullition.

During each sampling period, we also measured the diffusive flux of CO₂ and CH₄ at 12 of the sampling stations using a portable GHG analyzer attached to a floating acrylic chamber (Supporting Information Fig. S2b,c). We measured diffusion directly adjacent to the ebullition traps at 2–3 of the sampling stations in each transect. The analyzer measured the headspace gas concentration in the chamber every 1 s with a minimum contact time of 60 s (Off-Axis Integrated Cavity Output Spectroscopy Analyzer, GLA131 series; ABB). We calculated diffusive flux using the change in headspace gas concentration over the contact period using the following equation in which s is the rate of change in headspace gas concentration over time (ppm s⁻¹), V is the combined volume of the chamber and tubing internal and external to the analyzer (m³), SA is the surface area of the chamber (m²), P is pressure (atm), T is temperature (K), and R is the universal gas constant (m³ atm K⁻¹ mol⁻¹).

$$\text{flux} = \frac{s}{R \times T \times \frac{1}{P}} \times \frac{V}{SA}$$

Ebullition and changing light conditions during the diffusive flux measurements resulted in portions of the headspace concentration time series that were non-monotonic and nonlinear. We, therefore, estimated the most frequently occurring slope in the time series and used this value for our flux calculations. Briefly, we calculated the slope of every 10 sequential points in the time series and computed the maximum of the probability density function calculated using kernel density estimation. We checked these slopes visually to ensure they appropriately captured rates of diffusion.

To evaluate the daily contribution of the degassing pathway of emissions from our small reservoirs, we calculated the flux by taking the difference in CH₄ concentration of water collected near the dam intake (0.25 m below the water surface) and water collected from the dam outlet. We multiplied this difference by the dam discharge, which we estimated by measuring the time required to fill a known volume (Maeck et al. 2013). We divided this value by reservoir area to compare the contribution of degassing to those of other emissions pathways.

To measure dissolved gas concentrations to calculate degassing emissions, we followed the headspace equilibration protocol in Goodman (2019), but modified the purge gas to use ultra-zero air rather than ambient air. We also measured the dissolved gas concentrations in the inlet stream and at the bottom of the water column, 0.1 m from the sediment (Supporting Information Table S1). Briefly, we took three replicate, 60 mL bubble-free water samples using a Van Dorn bottle 0.25 m below the surface and 0.1 m from the sediment as well as from the inlet and outlet streams to estimate dissolved gas concentrations. On return to the lab, we introduced a 20 mL headspace of ultra-zero air and equilibrated the headspace by vigorously shaking the syringe for 5 min. We then injected 18 mL of the headspace into an evacuated 12 mL vial for gas

analysis. At the start of the sample run, we confirmed that both CO₂ and CH₄ concentrations in the purge gas were below the detection limit. We measured gas concentrations on an SRI Instruments 8610C Gas Chromatograph as described above and calculated the original dissolved gas concentration from the measured headspace gas concentrations.

Scaling point estimates to the reservoir surface

To estimate diffusion and ebullition from the entire surface of the reservoirs, we used sequential Gaussian simulation with simple kriging of our measured fluxes to generate equally probable realizations of emissions in unsampled areas from which to characterize the global uncertainty in our scaled emissions estimates (Delbari et al. 2009). For every sampling period in every reservoir, we generated 500 simulations of emissions across a 1-m² grid. We discarded the top and bottom 2.5% of realizations to estimate a 95% confidence interval. To generate the realizations, we used the kriging function in the gstat package (Pebesma 2004; Gräler et al. 2016). Because we did not have a CH₄ concentration corresponding to every measurement of gas volume from ebullition, we randomly assigned every volume measurement to a concentration measurement from the sampling event and simulated 25 realizations of ebullition using those concentrations. We repeated this procedure 20 times for a total of 500 simulations of ebullition per sampling event. To calculate rates of emissions from our interpolated estimates, we summed the values in each grid cell at a time point, multiplied that value by the time elapsed until the next sampling interval, summed across the sampling intervals, and then divided by reservoir area.

Drivers of diel patterns of emissions

To characterize diel patterns in CO₂ diffusion, CH₄ diffusion, and CH₄ ebullition, we plotted and visually inspected the fluxes interpolated with sequential Gaussian simulation across the sampling intervals. We then ran models explaining the measured point estimates of diffusive fluxes as a function of environmental variables we expected to relate to diel variation in diffusion, including DO at the top and bottom of the water column, wind speed, light, and temperature (Natchimuthu et al. 2016; Siczko et al. 2020; Rudberg et al. 2021; Hounshell et al. 2023). We recorded DO concentration 0.25 m below the water surface and 0.1 m from the sediment using a handheld meter (YSI Pro Plus) at two locations near the edge of the reservoir and two in the center during every sampling period. We took two 15 s integrated wind speed measurements using a handheld anemometer (HoldPeak 866) at approximately 1 m in height adjacent to the chamber during every diffusive flux measurement. We quantified light availability in two ways: (1) we measured illuminance every 15 min using a light logger installed on the bank of the reservoir where there was no tree cover (UA-002-64; Onset) and (2) we measured photosynthetically active radiation 0.5 m below the reservoir surface (Odyssey). We recorded temperature approximately every 0.5 m of depth using a chain of temperature loggers

installed at the deepest location in the reservoir (Onset). At this location, we also recorded DO every 15 min at 0.25 m below the water surface using a miniDOT (PME) to develop a continuous record of DO during our study period. We ran all subsets of a global linear mixed effects model predicting the diffusive flux of CO₂ or CH₄ using these variables (windspeed, surface water temperature, illuminance, and DO at the top and bottom of the water column-averaged across the four sampling locations). In each of these models, we scaled the predictors and used a random intercept for the sampling event, which was the site and date sampled. For the top models, we report unscaled parameter estimates (Supporting Information Table S2). We were unable to recover data from the PAR logger installed in Deans, so we ran separate models evaluating the explanatory power of PAR on CO₂ and CH₄ diffusion using data from the other three sites.

Effects of sampling locations

To evaluate the spatial patterns in CH₄ ebullition, we ran a mixed effects gamma regression model with a log link function to predict ebullition from (1) depth and (2) distance to inlet, with a random intercept for sampling event. Because we did not identify a temporal pattern in CH₄ ebullition, we aggregated ebullition across all sampling intervals in the 24-h sampling period for this analysis.

Simulating the consequences of sampling scheme

We conducted simulations using our measured flux data to evaluate the consequences of sampling emissions with less spatial and temporal intensity. We simulated the consequences of sampling one to 11 locations for diffusion and one to 24 locations for ebullition, while sampling the maximum number of times in the 24-h period. For every possible number of sampling locations, we generated 100 bootstrapped replicates for each pathway and calculated the number of replicates that fell within the 95% confidence interval of our interpolated emissions. We used 80% of simulations falling within the 95% confidence interval as an arbitrary threshold of estimation accuracy and calculated the number of sampling locations required to reach this threshold for each pathway of emissions (Robison et al. 2021). To calculate the mis-estimation associated with sampling fewer sites, we simulated every combination of one to four sampling locations where we measured both ebullition and diffusion. We took the estimation error to be the difference between the flux estimates generated from simulations using these locations and estimates generated using all of the sampled locations. To evaluate the consequences of sampling with less temporal intensity, we simulated sampling fluxes at every combination of one to two times during the day at the maximum number of sampling locations. To calculate the estimation error, we took the difference between these estimates and the fluxes estimated using all of the sampled times. To find the combinations of times that minimized estimation error across sites, we calculated the cumulative estimation error as the sum of the

errors from individual sites. Because Blue Herron had substantially different diel patterns from the other three sites, we determined the times that minimized cumulative estimation error separately for Blue Herron.

We conducted all analyses in R version 4.2.1 and produced figures using ggplot2 version 3.4.2 (Wickham 2016; R Core Team 2022). We ran the mixed models using the lmer and glmer functions in the lme4 package version 1.1-32 (Bates et al. 2015).

Results

Contributions of emissions pathways

Total interpolated emissions from the four reservoirs across the six sampling events ranged from 2.10 to 17.8 g CO₂-eq m⁻² d⁻¹ (Supporting Information Table S3). Each pathway of emissions (CO₂ diffusion, CH₄ diffusion, or CH₄ ebullition) contributed the most CO₂-eq in at least one reservoir on one sampling day (Fig. 1). CO₂ diffusion contributed the most CO₂-eq emissions from Deans and the 18 and 19 September Catfish sampling (50–77% of total CO₂-eq). During the 06 and 07 September Catfish sampling, CO₂ diffusion and CH₄ ebullition contributed approximately equally to total CO₂-eq emissions (46% and 49%, respectively). CH₄ ebullition contributed most from Sister (89% of total CO₂-eq) and CH₄ diffusion contributed most from Blue Herron (45% of total CO₂-eq), which was the only reservoir in which rates of CH₄ diffusion exceeded CH₄ ebullition (Fig. 1). The high rate of CH₄ diffusion in Blue Herron (the reservoir covered in duckweed) was consistent with its high surface CH₄ concentration of 98.7 μmol L⁻¹. The surface CH₄ concentrations for the other three sites were two orders of magnitude lower, ranging from 0.51 to 0.98 μmol L⁻¹ (Supporting Information Table S1). Despite the high concentration of dissolved CH₄ at Blue Herron, degassing emissions at this site contributed only 0.0003 g CH₄ m⁻² d⁻¹ or 0.008 g CO₂-eq m⁻² d⁻¹, less than 0.05% of total CO₂-eq emissions, due to the low discharge from the reservoir on the day of sampling (1.6 × 10⁻⁵ m³ s⁻¹). The concentration of CH₄ in the outlet exceeded the concentration near the dam intake on all but one other sampling date: Deans on the 16–17 August. Degassing emissions from this site were an order of magnitude lower than those from Blue Herron at 0.00003 g CH₄ m⁻² d⁻¹ or 0.0007 g CO₂-eq m⁻² d⁻¹, which was less than 0.001% of total CO₂-eq emissions from Deans on 16–17 August.

The high surface CH₄ concentration at Blue Herron is consistent with its persistent anoxia. During the sampling period, surface DO at the continuous sampling station near the center of the pond never exceeded 0.2 mg L⁻¹ (Supporting Information Figs. S3, S4). In contrast, the minimum surface DO concentration at the other three sites was 4.9 mg L⁻¹ in Deans, 7.2 mg L⁻¹ in Sister, and briefly 0.4 mg L⁻¹ in Catfish before rising to an average of 5.5 mg L⁻¹ (Supporting Information Fig. S3). Across all reservoirs, CO₂ diffusion ranged on average from -0.07 to

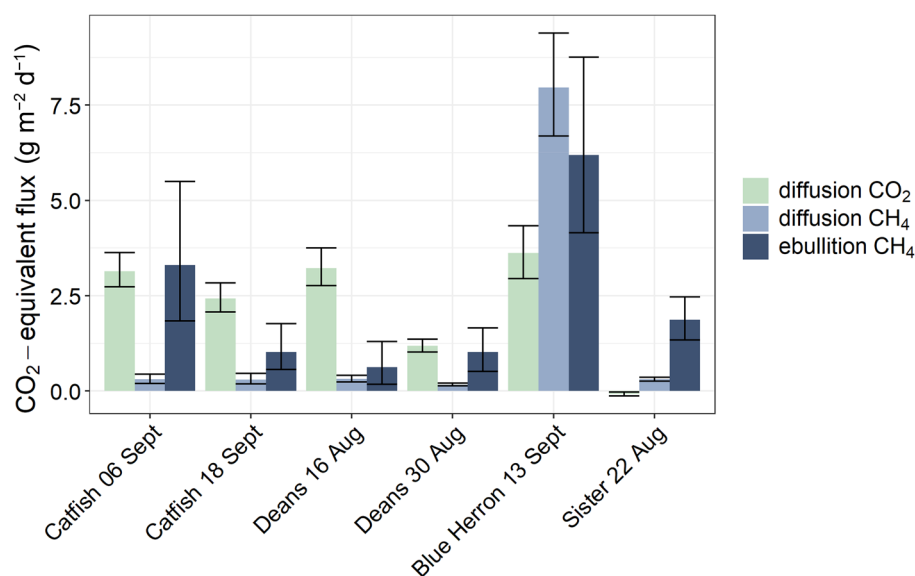


Fig. 1. CO₂-eq flux rates by emission pathway from estimates interpolated using sequential Gaussian simulation. Bars represent average values and error bars represent the simulated 95% confidence interval. The date listed is the start date of the 24-h sampling period.

3.62 g CO₂ m⁻² d⁻¹, CH₄ diffusion ranged from 0.01 to 0.29 g CH₄ m⁻² d⁻¹, and CH₄ ebullition from 0.02 to 0.23 g CH₄ m⁻² d⁻¹ (Supporting Information Table S3).

Diel patterns and drivers

We found no evidence of a diel pattern in CH₄ diffusion at Catfish, Deans, or Sister. At Blue Herron (the reservoir with duckweed), there was a distinct day–night pattern in CH₄ diffusion (g m⁻² h⁻¹), with the highest rates of diffusion at mid-day and declining rates in the late afternoon and night (Fig. 2). None of the models explaining CH₄ diffusion using environmental variables were more parsimonious than the intercept-only model. The next most parsimonious model ($\Delta\text{AICc} = 8.54$) included DO at the top of the water column, which was negatively associated with CH₄ diffusion (Supporting Information Fig. S5, $\beta = -0.001 \pm 0.0003$, $p = 0.003$, $t = -3.21$, $n = 573$, $R^2 = 0.17$).

Blue Herron also demonstrated a diel pattern of CO₂ diffusion distinct from those of the other reservoirs and from its diel pattern of CH₄ diffusion. The reservoir was a net sink for CO₂ in the late morning from 10:00 h to 13:00 h, after which it switched to being a net source (Fig. 2a). The rate of emissions increased through the night until it declined in the early morning hours. In contrast, in the other sites, there was only a slight dip in emissions at night (Fig. 2; Supporting Information Fig. S6). Because of the contrasting diel patterns of CH₄ and CO₂ diffusion, Blue Herron did not exhibit a diel pattern in total CO₂-eq emissions. In the other reservoirs, the pattern of lower CO₂ diffusion in the late afternoon and night did not result in a clear diel pattern in CO₂-eq emissions because of the lack of diel patterns in CH₄ diffusion and

ebullition; however, all reservoirs had variable CO₂-eq emissions throughout the day (Fig. 2).

The most parsimonious model explaining CO₂ diffusion included only DO at the top of the water column, which was negatively associated with CO₂ diffusion (Supporting Information Fig. S7, $\beta = -0.028 \pm 0.008$, $p = 0.008$, $t = -3.50$, $n = 573$, $R^2 = 0.14$) (Supporting Information Table S2). The next most parsimonious models were the intercept-only model ($\Delta\text{AICc} = 3.16$) and the model including water temperature at the top of the water column ($\Delta\text{AICc} = 5.00$). Temperature was negatively associated with CO₂ diffusion (Supporting Information Fig. S8, $\beta = -0.024 \pm 0.01$, $p = 0.033$, $n = 573$, $t = -2.49$, $R^2 = 0.12$), and this relationship strengthened when Blue Herron was excluded ($\beta = -0.036 \pm 0.006$, $p < 0.001$, $n = 477$, $t = -6.06$, $R^2 = 0.37$) (Supporting Information Table S2). Blue Herron had the highest CO₂ concentration (560 $\mu\text{mol L}^{-1}$) of the reservoirs, 4 times greater than the next highest concentration, which occurred in Catfish (138 $\mu\text{mol L}^{-1}$), and 14 times greater than the lowest concentration, which occurred in Sister (40.2 $\mu\text{mol L}^{-1}$) (Supporting Information Table S1).

Spatial variation

As predicted, both depth and distance to the inlet had negative associations with ebullition; however, only depth had a parameter estimate that did not overlap zero (inlet distance: -0.001 ± 0.003 , $n = 142$, $t = -0.41$, $p = 0.68$; depth: -0.30 ± 0.12 , $t = -2.4$, $p = 0.02$) and even combined these predictors explained little variation in ebullition ($R^2 = 0.03$). However, when Blue Herron was excluded, both predictors had greater negative associations with ebullition (inlet distance: -0.019 ± 0.0034 , $n = 118$, $t = -5.48$, $p < 0.001$; depth:

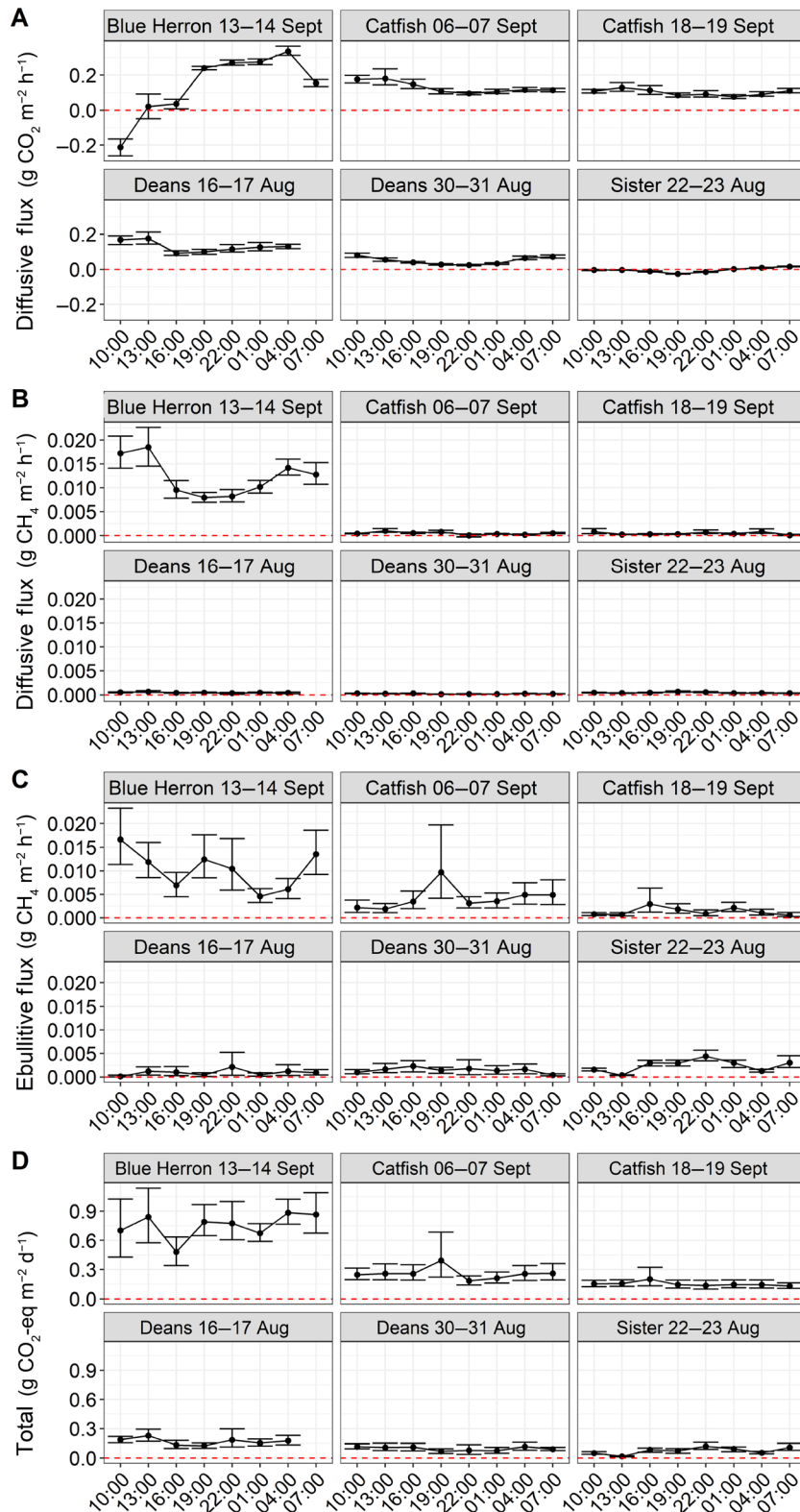


Fig. 2. Diel patterns in interpolated (A) CO₂ diffusion, (B) CH₄ diffusion, (C) CH₄ ebullition, and (D) total CO₂-eq emissions. Points represent average estimates and error bars represent the simulated 95% confidence interval. The times depicted for CH₄ ebullition are the end of the ebullition measurement period (i.e., when the gas volume was recorded). The 07:00 diffusive flux sampling for Deans on 16 August was delayed until 09:00 due to rain. These values were used to calculate total CO₂-eq flux over a 24-h period, but are not depicted here. See Supporting Information Fig. S6 for values depicted on free y-axis scales.

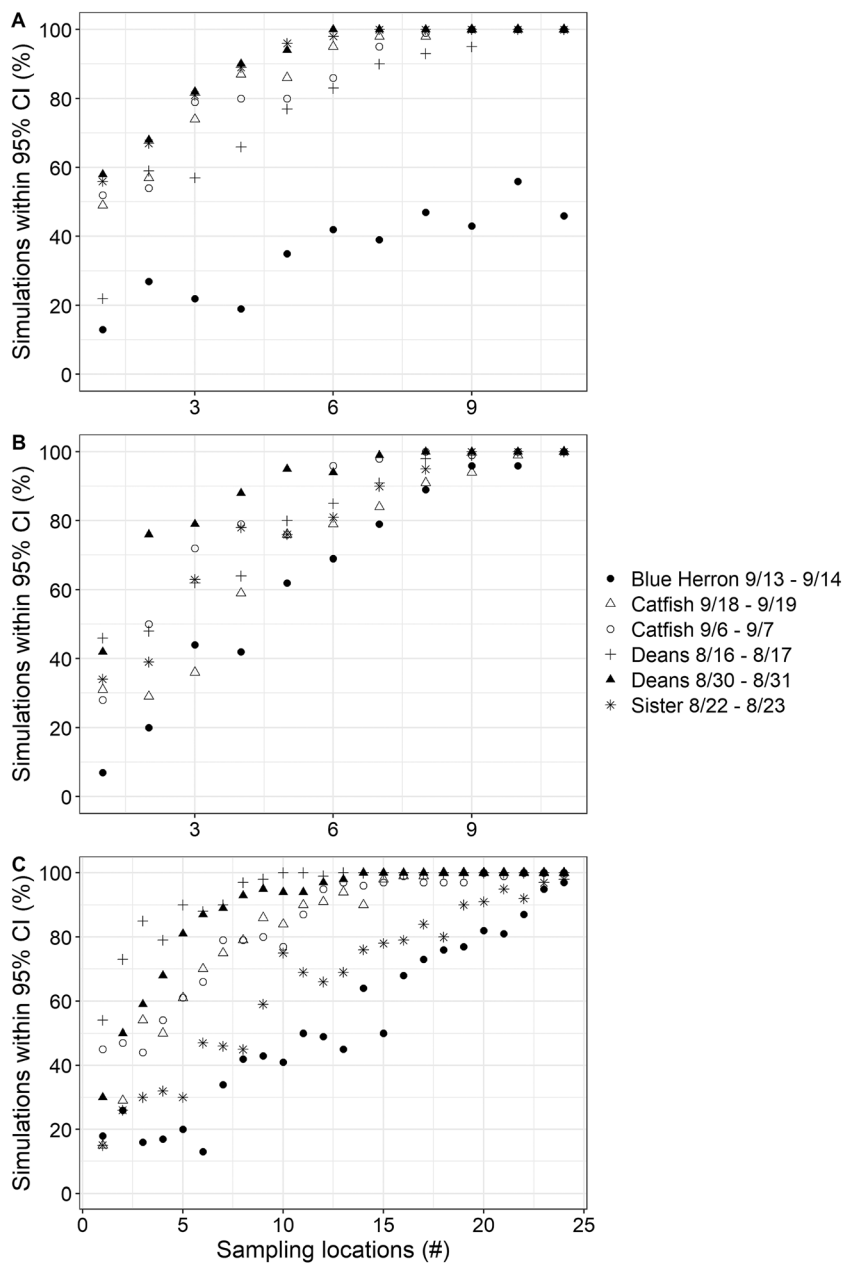


Fig. 3. The percentage of simulated samplings within the 95% confidence interval of the interpolated fluxes at iterative numbers of random sampling locations for **(A)** CO₂ diffusion, **(B)** CH₄ diffusion, **(C)** CH₄ ebullition.

-0.49 ± 0.11 , $n = 118$, $t = -4.35$, $p < 0.001$) and the model explained more of the total variation in ebullition ($R^2 = 0.44$). These parameter estimates correspond to a 39% decline in ebullition with every 1 m increase in depth and a 2% decline with every 1 m increase in distance from the reservoir inlet. Plots of CO₂ diffusion indicated a spatial pattern in Blue Herron, where every diffusive flux measurement was taken over duckweed (Supporting Information Fig. S2b). To confirm this spatial pattern, we calculated Moran's I to test for spatial autocorrelation for every sampling period and found that during six of eight time periods, measurements of CO₂ diffusion

were spatially autocorrelated, indicating that locations closer together in the reservoir had more similar fluxes than those far apart (Moran's I : 0.15–0.43) (Supporting Information Fig. S9). None of the other sites exhibited spatial patterns in CO₂ diffusion or had significant periods of spatial autocorrelation (Supporting Information Figs. S2b, S9).

Sampling scheme efficiency and accuracy

All sites except Blue Herron reached the arbitrary accuracy threshold (80% of simulations falling within the 95% confidence interval of the estimate calculated using all of the data)

when six locations were sampled for CO₂ diffusion and eight for CH₄ diffusion. Catfish and Deans reached the accuracy threshold for CH₄ ebullition at nine sampling locations, Sister at 17, and Blue Herron at 20 locations (Fig. 3). The estimation errors for sampling one to four locations in the reservoir, which is the difference between the fluxes calculated using a limited number of sampling locations and fluxes calculated using all of the locations, ranged from -10.43 to 13.47 g CO₂-eq m⁻² d⁻¹ and -85% to 366% of the total CO₂-eq flux.

Estimation errors for sampling only once during the day ranged from -5.61 to 2.56 g CO₂-eq m⁻² d⁻¹ or -78% to 45% of the total flux, but sampling at certain times or combinations of time substantially reduced estimation error. Sampling at 10:00 h and 22:00 h minimized the cumulative estimation error for CO₂ diffusion for the duckweed-free reservoirs: Catfish, Deans, and Sister. Other combinations of daytime and

nighttime sampling also had low cumulative estimation error (Fig. 4). The median estimation error from these individual reservoirs was 0.31 g CO₂ m⁻² d⁻¹, and the maximum estimation error was -1.05 g CO₂ m⁻² d⁻¹, 33% of the total diffusive CO₂ flux. Although there was no distinct diel pattern of CH₄ diffusion in these reservoirs (Supporting Information Fig. S6), there was variation in rates of emissions throughout the day. Diel variation in these reservoirs ranged from 0.001 g CH₄ m⁻² h⁻¹ to 0.008 g CH₄ m⁻² h⁻¹. As a result, the median estimation error from these individual reservoirs was 0.002 g CH₄ m⁻² d⁻¹ and the maximum estimation error was 0.01 g CH₄ m⁻² d⁻¹, 87% of the total diffusive CH₄ flux. Cumulative estimation error for CH₄ diffusion was minimized by sampling at 13:00 h and 22:00 h (Fig. 4).

For the duckweed-covered reservoir, Blue Herron, estimation error was minimized by sampling at 13:00 h and 04:00 h

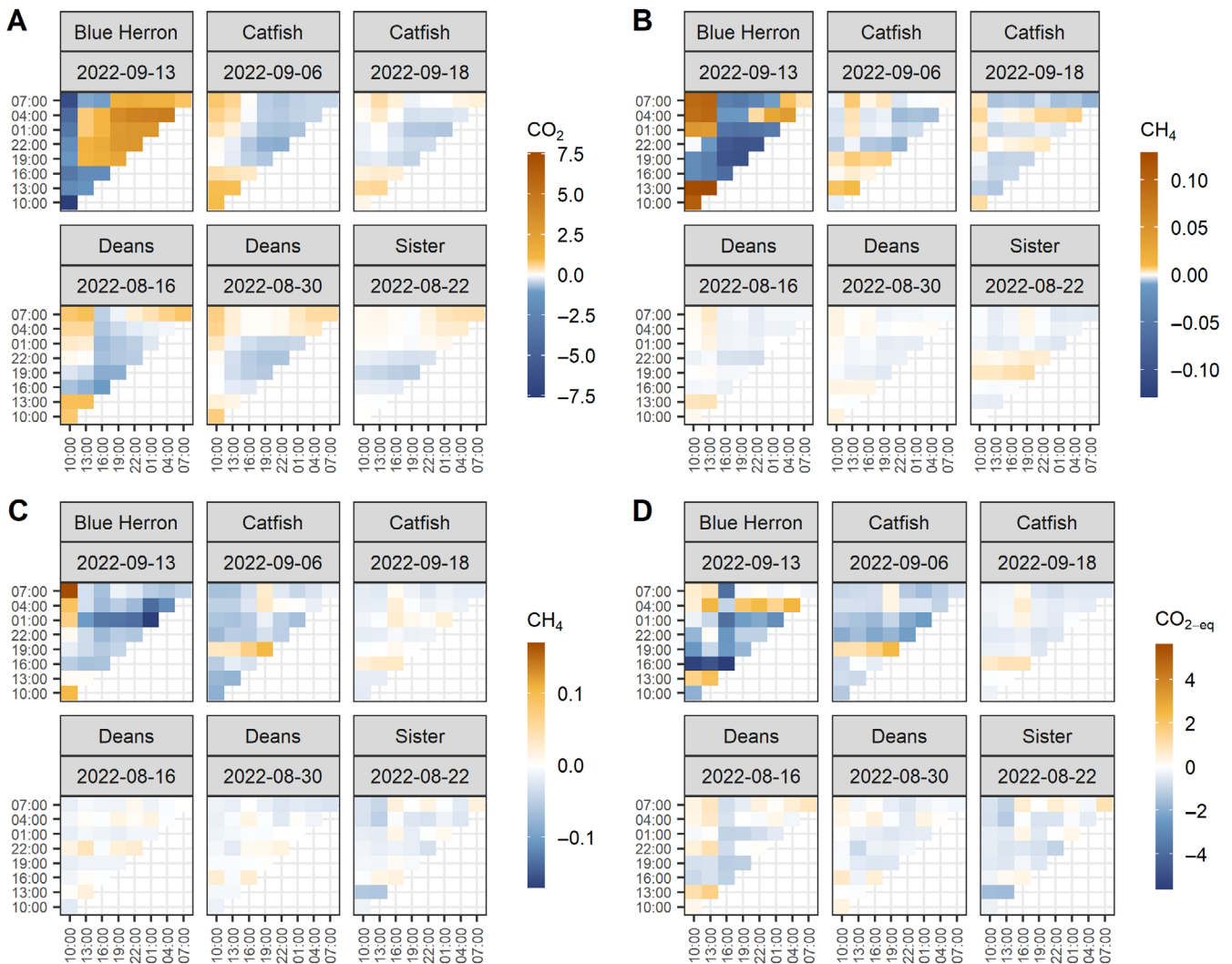


Fig. 4. (A) CO₂ diffusion (g CO₂ m⁻² d⁻¹), (B) CH₄ diffusion (g CH₄ m⁻² d⁻¹), (C) CH₄ ebullition (g CH₄ m⁻² d⁻¹), and (D) CO₂-eq (g CO₂-eq m⁻² d⁻¹) flux estimation error associated with different combinations of one to two sampling times throughout the day. The values along the diagonal represent sampling at only one time during the day.

($0.77 \text{ g CO}_2 \text{ m}^{-2} \text{ d}^{-1}$, 21% of the total diffusive CO_2 flux); however, sampling just once at 07:00 h was among the combinations of times with the lowest estimation error ($0.89 \text{ g CO}_2 \text{ m}^{-2} \text{ d}^{-1}$, 24% of the total diffusive CO_2 flux). In contrast, sampling at 10:00 h, which is the modal sampling hour for several GHG sampling efforts (Gómez-Gener et al. 2021; NEON 2023), had the highest estimation error for CO_2 diffusion ($-7.60 \text{ g CO}_2 \text{ m}^{-2} \text{ d}^{-1}$, 210% of the total diffusive CO_2 flux) (Fig. 4). For CH_4 diffusion, sampling at 10:00 h and 22:00 h minimized estimation error ($-0.0005 \text{ g CH}_4 \text{ m}^{-2} \text{ d}^{-1}$, 0.2% of the total diffusive CH_4 flux); however, like with CO_2 diffusion, sampling once at 07:00 h yielded low estimation error for CH_4 diffusion ($0.004 \text{ g CH}_4 \text{ m}^{-2} \text{ d}^{-1}$, 1.3% of the total diffusive CH_4 flux) (Fig. 4).

Discussion

Our results indicate that common practices of sampling small reservoir GHG emissions (i.e., not measuring ebullition, sampling at one time during the day, and sampling few locations in the reservoir) can lead to substantial misestimations of total CO_2 -eq flux from these ecosystems. Excluding ebullition from our estimates led to an underestimation of the total flux by -0.63 to $-6.19 \text{ g CO}_2\text{-eq m}^{-2} \text{ d}^{-1}$ or -15% to -89% of the total flux. Sampling only once during the day led to misestimation from -5.61 to $2.56 \text{ g CO}_2\text{-eq m}^{-2} \text{ d}^{-1}$ or -78% to 45% of the total flux. Sampling a few locations in the reservoir (four or fewer) led to misestimation between -10.43 to $13.47 \text{ g CO}_2\text{-eq m}^{-2} \text{ d}^{-1}$ or -366% to 85% of the total flux. Our results indicated that 6–20 sampling locations may be required for reasonable estimation accuracy, depending on the characteristics of a reservoir and the emissions pathway considered. We observed a distinct magnitude, spatial, and diel pattern of CH_4 and CO_2 emissions in the duckweed-covered reservoir compared to the other reservoirs, and the consequences of limited sampling were more severe in the duckweed reservoir. Our results can inform efforts to scale point measurements of emissions in space and in time in smaller waterbodies ($< 0.01 \text{ km}^2$), for which eddy covariance and other high-temporal resolution methods used for large reservoirs have limited effectiveness (Zhao et al. 2019).

Magnitude of emissions

Summer emissions from the four small reservoirs we sampled were within the range of values observed previously for reservoirs. Mean CO_2 emissions were higher ($2.25 \text{ g CO}_2 \text{ m}^{-2} \text{ d}^{-1}$) and mean CH_4 emissions ($0.145 \text{ g CH}_4 \text{ m}^{-2} \text{ d}^{-1}$) were slightly lower than the mean emissions from a global synthesis of reservoir emissions ($1.21 \text{ g CO}_2 \text{ m}^{-2} \text{ d}^{-1}$ and $0.161 \text{ g CH}_4 \text{ m}^{-2} \text{ d}^{-1}$); however, both gases were firmly within the range of previous observations (-1.30 to $9.66 \text{ g CO}_2 \text{ m}^{-2} \text{ d}^{-1}$ and 0 – $5.26 \text{ g CH}_4 \text{ m}^{-2} \text{ d}^{-1}$) (Deemer et al. 2016). Notably, only two of the 144 reservoirs with diffusive CH_4 fluxes measurements in Deemer et al. (2016) had a

higher diffusive CH_4 flux than the duckweed reservoir ($0.29 \text{ g CH}_4 \text{ m}^{-2} \text{ d}^{-1}$), and only 8 of 54 had a higher ebullitive flux of CH_4 than the duckweed reservoir ($0.23 \text{ g CH}_4 \text{ m}^{-2} \text{ d}^{-1}$). However, we only measured emissions during the summer, and prior evidence of seasonal patterns in emissions suggests that annual diffusive and ebullitive fluxes of CH_4 may be lower than the values reported here (van Bergen et al. 2019). Comparing our findings to waterbodies in the same size class that were not formed by dams, we found both a higher mean CO_2 flux (2.25 vs. $0.933 \text{ g CO}_2 \text{ m}^{-2} \text{ d}^{-1}$) and CH_4 flux (0.145 vs. $0.010 \text{ g CH}_4 \text{ m}^{-2} \text{ d}^{-1}$) from our small reservoirs (Holgerson and Raymond 2016).

A limitation of our ability to ascribe the patterns in gas fluxes we observed to the presence of duckweed is that duckweed was only abundant in one of our reservoirs. However, the patterns we observed were consistent with the overriding control of emissions by floating macrophytes which has been observed in previous studies (Bastviken et al. 2010; Rabaey and Cotner 2022). The rate of CO_2 -eq emissions ($\text{g m}^{-2} \text{ d}^{-1}$) in the duckweed reservoir was, on average, 5.5 times greater than the other three reservoirs, and CH_4 emissions from this site accounted for 80% of total CO_2 -eq emissions. Duckweed likely elevated CH_4 emissions by limiting O_2 exchange across the air–water interface and loading labile organic carbon to the sediments, generating persistent anoxia and fueling methanogenesis (Morris and Barker 1976; Kosten et al. 2016; Rabaey and Cotner 2022).

Although small reservoirs have the capacity to emit large quantities of GHGs, they also have the capacity to bury large quantities of carbon. One study found that organic carbon burial rates in eutrophic, midwestern U.S. reservoirs were three orders of magnitude higher than mean burial rates in temperate forests (Downing et al. 2008). These burial rates far exceeded rates of CO_2 diffusion from these reservoirs (Pacheco et al. 2014). In contrast, in a temperate, eutrophic pond, carbon burial was only 7.4% of the annual emissions (van Bergen et al. 2019). The carbon balance of our small reservoirs is unknown. While duckweed is very labile, its breakdown in the sediments of the duckweed reservoir may be slow. Our duckweed-dominated reservoir was anoxic for much of the year (unpublished data), potentially resulting in the slow breakdown of duckweed biomass and subsequent carbon storage. Additional work on carbon burial is needed to understand the role of small reservoirs in landscape carbon balance (Holgerson et al. 2024).

Diel patterns

The duckweed-free reservoirs demonstrated slight declines in CO_2 diffusion at night. In contrast to studies in larger reservoirs, this pattern did not appear to be associated with higher daytime wind speeds; however, we observed a relatively small range of wind speeds (0 – 7.2 m s^{-1} , mean: 0.4 m s^{-1}) and it is possible that a positive relationship between wind speed and CO_2 diffusion would be apparent with windier conditions

(Crusius and Wanninkhof 2003). Wind may also be a less important driver of CO₂ diffusion in these reservoirs because of their small area and insulation by trees (Vachon and Prairie 2013). In the duckweed reservoir, the net uptake of CO₂ from 10:00 h to 13:00 h is consistent with a mid-morning peak in CO₂ fixation, which was previously observed in a small lake covered in a different duckweed species (*Lemna minor*) (Filbin and Hough 1985). Although solar radiation may be more intense later in the day, an afternoon depression in rates of CO₂ fixation may occur due to photoinhibition and photorespiration (Filbin and Hough 1985), consistent with the increase in CO₂ emissions we observed in the afternoon in the duckweed reservoir. In the duckweed-free reservoirs, the dominant primary producers were submerged below the water surface. Attenuation of light through the water column may have reduced the strength of photoinhibition, resulting in a later peak in autotrophic CO₂ uptake and a minimum in CO₂ emissions (Walsby 1997). Although we did not observe a relationship between CO₂ emissions and PAR measured at a fixed station in the reservoir, we did observe a negative relationship between CO₂ emissions and surface DO, which is consistent with autotrophs driving diel patterns of CO₂ emissions, as in the mechanism proposed above. Our simulations indicated that sampling once during the day and once at night in the duckweed-free reservoirs resulted in low estimation errors, with the smallest errors resulting from sampling at 10:00 h and 22:00 h. Estimation errors in the duckweed reservoir were much larger but were minimized by sampling at 13:00 h and 04:00 h or at 07:00 h alone. If we had sampled at 10:00 h only, which is the modal sampling time of prior efforts (Gómez-Gener et al. 2021; NEON 2023), we could have concluded that the duckweed reservoir was a sink for CO₂ when it was a source, emphasizing the importance of accounting for diel patterns of emissions.

The duckweed reservoir was the only site that exhibited a diel pattern of CH₄ diffusion. It had high rates of diffusion in the late morning and early afternoon (10:00–13:00 h), followed by a sharp decline in the late afternoon and persistently low rates through the night (16:00–01:00 h), and rising again in the early morning (04:00–07:00 h). In contrast to findings in other lentic waterbodies, diel variations in wind speed did not explain the higher daytime diffusive CH₄ fluxes we observed (Liu et al. 2017; Siczko et al. 2020). In this reservoir, the peak in light coincided with the peak in surface DO, indicating a possible contribution by duckweed to surface DO. CH₄ oxidation during these periods of elevated DO may have decreased CH₄ diffusion from the reservoir surface (Kosten et al. 2016). Consistent with this mechanism, the strongest association between CH₄ diffusion and an environmental variable across all reservoirs was the negative association with surface DO; however, the model including surface DO explained little variation ($R^2 = 0.17$), indicating that other mechanisms may be generating diel patterns in CH₄ diffusion, alone or in conjunction with CH₄ oxidation. Estimation errors

for CH₄ diffusion in the duckweed reservoir were minimized with sampling at 10:00 h and 22:00 h or at 07:00 h alone.

The amplitude of diel CO₂ emissions in the duckweed reservoir (0.55 g CO₂ m⁻² h⁻¹) was at the high end of the range observed in previous studies of sub-daily emissions from lentic inland waters. A similar amplitude (0.56 g CO₂ m⁻² h⁻¹) was observed in ponds in the subarctic wetland region of the Hudson Bay Lowlands, Canada, where CO₂ emissions were attributed to degrading peat (Hamilton et al. 1994). The duckweed reservoir amplitude was 2.6 times higher than that observed in a larger eutrophic reservoir (0.119 km²) (Hounshell et al. 2023). We observed the lowest amplitude in Sister, which was an order of magnitude lower (0.042 g CO₂ m⁻² h⁻¹) than the duckweed reservoir. The diel variation in CO₂ emissions from Sister was similar to the minimum amplitude reported in a synthesis of CO₂ emissions from 13 northern latitude lakes and reservoirs, which ranged widely in size, nutrient, and humic states (Golub et al. 2021). For CH₄ diffusion, the duckweed reservoir was the only reservoir that exhibited a diel pattern. Like CO₂ diffusion, the amplitude of diel CH₄ diffusion from the duckweed reservoir (0.011 g CH₄ m⁻² h⁻¹) was at the high end of the range of previous observations. It was equal to the amplitude of CH₄ emissions measured over dense patches of water hyacinth (*Pontederia* sp.) in shallow lakes in the Pantanal, Brazil (Bastviken et al. 2010). The high amplitude of variation for CO₂ and CH₄ diffusion in the duckweed reservoir highlights the special consideration that sub-daily, temporal variation may merit in characterizing emissions from smaller, floating macrophyte-covered reservoirs. The diel patterns we observed are consistent with substantial autotrophic control of emissions and were consequential for estimating total emissions from the duckweed reservoir. However, we only sampled emissions during the summer, and lower primary producer biomass and temperature in the winter may result in lower diel fluctuations in diffusion (Ollivier et al. 2019b). Sub-daily variation, therefore, may be less important for emissions estimates at other times of the year. Further investigation of seasonal changes in diel patterns of emissions from small reservoirs merits further study.

Spatial patterns

In the duckweed-free reservoirs, we observed a decline in daily rates of CH₄ ebullition with increasing distance from the inlet and depth, consistent with patterns observed in larger reservoirs (Beaulieu et al. 2016; McClure et al. 2020). Terrestrial organic matter delivered by the inlet streams may have dominated organic matter inputs, creating a pattern of higher sediment organic matter availability near the reservoir inlet. In these reservoirs, CH₄ ebullition declined by 2% for every 1 m increase in distance from the reservoir inlet and 39% for every 1 m increase in depth. However, in the duckweed reservoir, the extensive macrophyte coverage may have more evenly distributed organic matter across the reservoir

sediments and persistent water column anoxia may have reduced rates of CH₄ oxidation, eliminating the decline in ebullition with increasing inlet distance and depth that we observed in the duckweed-free reservoirs. In general, more sampling locations were required to accurately estimate fluxes in the duckweed reservoir than in the duckweed-free reservoirs. A high degree of estimation accuracy was reached in the duckweed-free reservoirs when at least 6 locations were sampled for CO₂ diffusion, 8 locations for CH₄ diffusion, and 17 locations were sampled for ebullition. In the duckweed reservoir, 12 or more sampling locations were required to estimate CO₂ diffusion, 8 locations for CH₄ diffusion, and 20 locations for CH₄ ebullition.

Extrapolation to other small reservoirs

To interpret the implications of our findings, it is important to consider whether the differences we observed between the duckweed-dominated and duckweed-free reservoirs can be extrapolated to small reservoirs with high biomass of other dominant primary producers. Elevated diel variation in CO₂ emissions has been linked to photosynthetic uptake by large stands of submerged and emergent macrophytes, as well as blooms of phytoplankton (Maberly 1996; Kragh et al. 2017; Golub et al. 2021). However, the exact diel patterns of emissions may differ by dominant primary producer. For example, primary producers differ in their susceptibility to photo-inhibition (Wetzel 2001), which could impact diel patterns of photosynthesis, CO₂ supply, and flux. Because photosynthesis can control CO₂ fluxes, we may also expect greater spatial patterns of CO₂ emissions in small reservoirs with high primary producer biomass, as observed in the duckweed reservoir. However, primary production may not be a major driver of CO₂ emissions if a reservoir receives large external inputs of CO₂ (e.g., in groundwater), even when primary producer biomass is high; in this case, diel and spatial patterns of CO₂ diffusion may not be apparent (van Bergen et al. 2019).

Diel patterns of CH₄ diffusion can arise in reservoirs dominated by primary producers other than duckweed, although the patterns and mechanisms may differ (Hamilton et al. 1994; Bastviken et al. 2010). We expect that other floating macrophytes are likely to behave similarly to duckweed in enhancing CH₄ oxidation, potentially generating a pattern of lower CH₄ emissions when surface DO is high due to photosynthesis (Kosten et al. 2016; Iguchi et al. 2019). In reservoirs dominated by rooted macrophytes, vegetation-mediated emissions could modify these temporal patterns by transporting CH₄ from the water column or sediment pore water to the atmosphere (Whiting and Chanton 1996; Bolpagni et al. 2007). The impact of high phytoplankton biomass on diel patterns of CH₄ fluxes is uncertain; previous studies have identified both the presence and absence of a diel pattern of CH₄ fluxes in lentic ecosystems with high phytoplankton biomass (van Bergen et al. 2019; Waldo et al. 2021). Primary producer identity may be an important factor in determining diel patterns of CH₄ diffusion, and

floating macrophyte-dominated small reservoirs may exhibit distinct patterns compared to those dominated by other types of macrophytes and algae.

Conclusion

Several recent inventories of GHG emissions from inland waters have specifically identified the need for emissions estimates from abundant small reservoirs (Deemer and Holgeron 2021; Pilla et al. 2022; Lauerwald et al. 2023). By intensively sampling small reservoirs in space and time, we identified key considerations for efficiently estimating emissions from point measurements. Our results indicate that 07:00 h, just after dawn, may be an efficient time to sample while sampling later in the morning or early afternoon may result in greater estimation errors due to diel patterns of CO₂ and CH₄ diffusion. Sampling 6–20 locations in the reservoir may be required for reasonable estimation accuracy. Our results suggest that more sampling locations may be required to characterize emissions from duckweed-covered reservoirs than duckweed-free reservoirs. Selecting sampling locations for ebullition with varying depth and distance to the reservoir inlet may also improve estimation accuracy, as our results indicate that ebullition declined with increasing depth and declined with increasing distance to the inlet in all sites except for the duckweed-covered reservoir. These results can inform efforts to characterize emissions from small reservoirs and include them in regional and global inventories of GHG emissions from inland waters.

Accurate emissions estimates can also facilitate the identification of drivers of high GHG emissions, which can reveal management strategies to reduce emissions from these systems (Malerba et al. 2022; Nijman et al. 2022). For example, our results highlight management methods to reduce duckweed coverage as potential strategies to reduce GHG emissions from small reservoirs. While the impact of duckweed management on small reservoir GHG emissions has not, to our knowledge, been evaluated, duckweed removal from small ponds and reservoirs is a common practice with the potential to enhance DO content and reduce organic matter loading (Lembi 2009), decreasing rates of methanogenesis. Duckweed harvest from high-nutrient ponds has even been recommended as a method to generate feed and fertilizer while reducing stream nitrogen loads from farms (Femeena et al. 2022), highlighting a potential synergy between nutrient and GHG management. With over 2 million small reservoirs in the continental United States alone, opportunities to reduce GHG emissions from small reservoirs are abundant.

Data availability statement

The data and code used to generate all analyses and figures can be found in the following repository: <https://zenodo.org/doi/10.5281/zenodo.10573817>.

References

- Bastviken, D., J. J. Cole, M. L. Pace, and M. C. Van de Bogert. 2008. Fates of methane from different lake habitats: Connecting whole-lake budgets and CH₄ emissions. *J. Geophys. Res.: Biogeosci.* **113**: G02024. doi:10.1029/2007JG000608
- Bastviken, D., A. L. Santoro, H. Marotta, L. Q. Pinho, D. F. Calheiros, P. Crill, and A. Enrich-Prast. 2010. Methane emissions from Pantanal, South America, during the low water season: Toward more comprehensive sampling. *Environ. Sci. Technol.* **44**: 5450–5455. doi:10.1021/es1005048
- Bates, D., M. Mächler, B. Bolker, and S. Walker. 2015. Fitting linear mixed-effects models using lme4. *J. Stat. Softw.* **67**: 1–48. doi:10.18637/jss.v067.i01
- Beaulieu, J. J., M. G. McManus, and C. T. Nietch. 2016. Estimates of reservoir methane emissions based on a spatially balanced probabilistic-survey. *Limnol. Oceanogr.* **61**: S27–S40. doi:10.1002/lno.10284
- Bolpagni, R., E. Pierobon, D. Longhi, D. Nizzoli, M. Bartoli, M. Tomaselli, and P. Viaroli. 2007. Diurnal exchanges of CO₂ and CH₄ across the water–atmosphere interface in a water chestnut meadow (*Trapa natans* L.). *Aquat. Bot.* **87**: 43–48. doi:10.1016/j.aquabot.2007.02.002
- Boudreau, B. P. 2012. The physics of bubbles in surficial, soft, cohesive sediments. *Mar. Pet. Geol.* **38**: 1–18. doi:10.1016/j.marpetgeo.2012.07.002
- Cole, J. J., and N. F. Caraco. 1998. Atmospheric exchange of carbon dioxide in a low-wind oligotrophic lake measured by the addition of SF₆. *Limnol. Oceanogr.* **43**: 647–656. doi:10.4319/lo.1998.43.4.0647
- Crusius, J., and R. Wanninkhof. 2003. Gas transfer velocities measured at low wind speed over a lake. *Limnol. Oceanogr.* **48**: 1010–1017. doi:10.4319/lo.2003.48.3.1010
- Deemer, B. R., and M. A. Holgerson. 2021. Drivers of methane flux differ between lakes and reservoirs, complicating global upscaling efforts. *J. Geophys. Res.: Biogeosci.* **126**: e2019JG005600. doi:10.1029/2019JG005600
- Deemer, B. R., and others. 2016. Greenhouse gas emissions from reservoir water surfaces: A new global synthesis. *BioScience* **66**: 949–964. doi:10.1093/biosci/biw117
- Delbari, M., P. Afrasiab, and W. Loiskandl. 2009. Using sequential Gaussian simulation to assess the field-scale spatial uncertainty of soil water content. *CATENA* **79**: 163–169. doi:10.1016/j.catena.2009.08.001
- Downing, J. A. 2010. Emerging global role of small lakes and ponds: Little things mean a lot. *Limnetica* **29**: 9–24. doi:10.23818/limn.29.02
- Downing, J. A., J. J. Cole, J. J. Middelburg, R. G. Striegl, C. M. Duarte, P. Kortelainen, Y. T. Prairie, and K. A. Laube. 2008. Sediment organic carbon burial in agriculturally eutrophic impoundments over the last century. *Glob. Biogeochem. Cycles* **22**: GB1018. doi:10.1029/2006GB002854
- Femeena, P. V., G. R. House, and R. A. Brennan. 2022. Creating a circular nitrogen bioeconomy in agricultural systems through nutrient recovery and upcycling by microalgae and duckweed: Past efforts and future trends. *J. ASABE* **65**: 327–346. doi:10.13031/ja.14891
- Filbin, G. J., and R. A. Hough. 1985. Photosynthesis, photorespiration, and productivity in *Lemna minor* L. *Limnol. Oceanogr.* **30**: 322–334. doi:10.4319/lo.1985.30.2.0322
- Ford, P. W., P. I. Boon, and K. Lee. 2002. Methane and oxygen dynamics in a shallow floodplain lake: The significance of periodic stratification. *Hydrobiologia* **485**: 97–110. doi:10.1023/A:1021379532665
- Forster, P. T., and others. 2021. The Earth’s energy budget, climate feedbacks, and climate sensitivity, p. 923–1054. *In* Climate change 2021: The physical science basis. Contribution of working group I to the sixth assessment report of the intergovernmental panel on climate change. Cambridge Univ. Press.
- Friedl, G., and A. Wüest. 2002. Disrupting biogeochemical cycles—Consequences of damming. *Aquat. Sci.* **64**: 55–65. doi:10.1016/0025-326x(91)90729-c
- Golub, M., and others. 2021. New insights into diel to inter-annual variation in carbon dioxide emissions from lakes and reservoirs. *ESS Open Arch.* doi:10.1002/essoar.10507313.1
- Gómez-Gener, L., and others. 2021. Global carbon dioxide efflux from rivers enhanced by high nocturnal emissions. *Nat. Geosci.* **14**: 289–294. doi:10.1038/s41561-021-00722-3
- Goodman, K. 2019. AOS Protocol and Procedure: SDG—Surface Water Dissolved Gas Sampling.
- Gotvald, A. 2017. Methods for estimating selected low-flow frequency statistics and mean annual flow for ungaged locations on streams in North Georgia. USGS numbered series 2017-5001. U.S. Geological Survey. doi:10.3133/sir20175001
- Gräler, B., E. Pebesma, and G. Heuvelink. 2016. Spatio-temporal interpolation using gstat. *R J.* **8**: 204–218. doi:10.32614/RJ-2016-014
- Grinham, A., M. Dunbabin, D. Gale, and J. Udy. 2011. Quantification of ebullitive and diffusive methane release to atmosphere from a water storage. *Atmos. Environ.* **45**: 7166–7173. doi:10.1016/j.atmosenv.2011.09.011
- Grinham, A., S. Albert, N. Deering, M. Dunbabin, D. Bastviken, B. Sherman, C. E. Lovelock, and C. D. Evans. 2018. The importance of small artificial water bodies as sources of methane emissions in Queensland, Australia. *Hydrol. Earth Syst. Sci.* **22**: 5281–5298. doi:10.5194/hess-22-5281-2018
- Hamilton, J. D., C. A. Kelly, J. W. M. Rudd, R. H. Hesslein, and N. T. Roulet. 1994. Flux to the atmosphere of CH₄ and CO₂ from wetland ponds on the Hudson Bay lowlands (HBLs). *J. Geophys. Res. Atmos.* **99**: 1495–1510. doi:10.1029/93JD03020
- Harrison, J. A., B. R. Deemer, M. K. Birchfield, and M. T. O’Malley. 2017. Reservoir water-level drawdowns accelerate

- and amplify methane emission. *Environ. Sci. Technol.* **51**: 1267–1277. doi:10.1021/acs.est.6b03185
- Harvey, J. W., and N. M. Schmadel. 2021. The river corridor's evolving connectivity of lotic and lentic waters. *Front. Water* **2**: 580727. doi:10.3389/frwa.2020.580727
- Holgerson, M. A., and P. A. Raymond. 2016. Large contribution to inland water CO₂ and CH₄ emissions from very small ponds. *Nat. Geosci.* **9**: 222–226. doi:10.1038/ngeo2654
- Holgerson, M. A., N. E. Ray, and C. Russ. 2024. High rates of carbon burial linked to autochthonous production in artificial ponds. *Limnol. Oceanogr.: Lett.* **9**: 43–51. doi:10.1002/lol2.10351
- Hounshell, A. G., B. M. D'Acunha, A. Breef-Pilz, M. S. Johnson, R. Q. Thomas, and C. C. Carey. 2023. Eddy covariance data reveal that a small freshwater reservoir emits a substantial amount of carbon dioxide and methane. *J. Geophys. Res.: Biogeosci.* **128**: e2022JG007091. doi:10.1029/2022JG007091
- Iguchi, H., R. Umeda, H. Taga, T. Oyama, H. Yurimoto, and Y. Sakai. 2019. Community composition and methane oxidation activity of methanotrophs associated with duckweeds in a fresh water lake. *J. Biosci. Bioeng.* **128**: 450–455. doi:10.1016/j.jbiosc.2019.04.009
- Kemenes, A., B. R. Forsberg, and J. M. Melack. 2007. Methane release below a tropical hydroelectric dam. *Geophys. Res. Lett.* **34**: L12809. doi:10.1029/2007GL029479
- Kosten, S., M. Piñeiro, E. de Goede, J. de Klein, L. P. M. Lamers, and K. Ettwig. 2016. Fate of methane in aquatic systems dominated by free-floating plants. *Water Res.* **104**: 200–207. doi:10.1016/j.watres.2016.07.054
- Kragh, T., M. R. Andersen, and K. Sand-Jensen. 2017. Profound afternoon depression of ecosystem production and nighttime decline of respiration in a macrophyte-rich, shallow lake. *Oecologia* **185**: 157–170. doi:10.1007/s00442-017-3931-3
- Lauerwald, R., and others. 2023. Inland water greenhouse gas budgets for RECCAP2: 1. State-of-the-art of global scale assessments. *Glob. Biogeochem. Cycles* **37**: e2022GB007657. doi:10.1029/2022GB007657
- Lembi, C. A. 2009. Control of duckweed and watermeal. APM-2-W. APM-2-W Purdue Extension.
- Linkhorst, A., J. R. Paranaíba, R. Mendonça, D. Rudberg, T. DelSontro, N. Barros, and S. Sobek. 2021. Spatially resolved measurements in tropical reservoirs reveal elevated methane ebullition at river inflows and at high productivity. *Glob. Biogeochem. Cycles* **35**: e2020GB006717. doi:10.1029/2020GB006717
- Liu, L., M. Xu, R. Li, and R. Shao. 2017. Timescale dependence of environmental controls on methane efflux from Poyang Hu, China. *Biogeosciences* **14**: 2019–2032. doi:10.5194/bg-14-2019-2017
- Maberly, S. C. 1996. Diel, episodic and seasonal changes in pH and concentrations of inorganic carbon in a productive lake. *Freshw. Biol.* **35**: 579–598. doi:10.1111/j.1365-2427.1996.tb01770.x
- Maeck, A., T. Delsontro, D. F. McGinnis, H. Fischer, S. Flury, M. Schmidt, P. Fietzek, and A. Lorke. 2013. Sediment trapping by dams creates methane emission hot spots. *Environ. Sci. Technol.* **47**: 8130–8137. doi:10.1021/es4003907
- Malerba, M. E., D. B. Lindenmayer, B. C. Scheele, P. Waryszak, I. N. Yilmaz, L. Schuster, and P. I. Macreadie. 2022. Fencing farm dams to exclude livestock halves methane emissions and improves water quality. *Glob. Change Biol.* **28**: 4701–4712. doi:10.1111/gcb.16237
- McClure, R. P., M. E. Lofton, S. Chen, K. M. Krueger, J. C. Little, and C. C. Carey. 2020. The magnitude and drivers of methane ebullition and diffusion vary on a longitudinal gradient in a small freshwater reservoir. *J. Geophys. Res.: Biogeosci.* **125**: e2019JG005205. doi:10.1029/2019JG005205
- Morris, P. F., and W. G. Barker. 1976. Oxygen transport rates through mats of *Lemna minor* and *Wolffia* sp. and oxygen tension within and below the mat. *Can. J. Bot.* **55**: 1926–1932. doi:10.1139/b77-220
- Natchimuthu, S., B. Panneer Selvam, and D. Bastviken. 2014. Influence of weather variables on methane and carbon dioxide flux from a shallow pond. *Biogeochemistry* **119**: 403–413. doi:10.1007/s10533-014-9976-z
- Natchimuthu, S., I. Sundgren, M. Gålfalk, L. Klemedtsson, P. Crill, Å. Danielsson, and D. Bastviken. 2016. Spatio-temporal variability of lake CH₄ fluxes and its influence on annual whole lake emission estimates. *Limnol. Oceanogr.* **61**: S13–S26. doi:10.1002/lno.10222
- NEON. 2023. Dissolved gases in surface water (DP1.20097.001).
- Nijman, T. P. A., M. Lemmens, M. Lurling, S. Kosten, C. Welte, and A. J. Veraart. 2022. Phosphorus control and dredging decrease methane emissions from shallow lakes. *Sci. Total Environ.* **847**: 157584. doi:10.1016/j.scitotenv.2022.157584
- Nimick, D. A., C. H. Gammons, and S. R. Parker. 2011. Diel biogeochemical processes and their effect on the aqueous chemistry of streams: A review. *Chem. Geol.* **283**: 3–17. doi:10.1016/j.chemgeo.2010.08.017
- Ollivier, Q. R., D. T. Maher, C. Pitfield, and P. I. Macreadie. 2019a. Punching above their weight: Large release of greenhouse gases from small agricultural dams. *Glob. Change Biol.* **25**: 721–732. doi:10.1111/gcb.14477
- Ollivier, Q. R., D. T. Maher, C. Pitfield, and P. I. Macreadie. 2019b. Winter emissions of CO₂, CH₄, and N₂O from temperate agricultural dams: Fluxes, sources, and processes. *Ecosphere* **10**: e02914. doi:10.1002/ecs2.2914
- Pacheco, F., F. Roland, and J. Downing. 2014. Eutrophication reverses whole-lake carbon budgets. *Inland Waters* **4**: 41–48. doi:10.5268/IW-4.1.614
- Paranaíba, J. R., N. Barros, R. Mendonça, A. Linkhorst, and A. Isidorova. 2018. Spatially resolved measurements of CO₂ and CH₄ concentration and gas-exchange velocity highly

- influence carbon-emission estimates of reservoirs. *Environ. Sci. Technol.* **52**: 607–615. doi:[10.1021/acs.est.7b05138](https://doi.org/10.1021/acs.est.7b05138)
- Peacock, M., J. Audet, S. Jordan, J. Smeds, and M. B. Wallin. 2019. Greenhouse gas emissions from urban ponds are driven by nutrient status and hydrology. *Ecosphere* **10**: e02643. doi:[10.1002/ecs2.2643](https://doi.org/10.1002/ecs2.2643)
- Pebesma, E. J. 2004. Multivariable geostatistics in S: The gstat package. *Comput. Geosci.* **30**: 683–691. doi:[10.1016/j.cageo.2004.03.012](https://doi.org/10.1016/j.cageo.2004.03.012)
- Pilla, R. M., N. A. Griffiths, L. Gu, S.-C. Kao, R. McManamay, D. M. Ricciuto, and X. Shi. 2022. Anthropogenically driven climate and landscape change effects on inland water carbon dynamics: What have we learned and where are we going? *Glob. Change Biol.* **28**: 5601–5629. doi:[10.1111/gcb.16324](https://doi.org/10.1111/gcb.16324)
- R Core Team. 2022. R: A language and environment for statistical computing.
- Rabaey, J., and J. Cotner. 2022. Pond greenhouse gas emissions controlled by duckweed coverage. *Front. Environ. Sci.* **10**: 889289. doi:[10.3389/fenvs.2022.889289](https://doi.org/10.3389/fenvs.2022.889289)
- Robison, A. L., W. M. Wollheim, B. Turek, C. Bova, C. Snay, and R. K. Varner. 2021. Spatial and temporal heterogeneity of methane ebullition in lowland headwater streams and the impact on sampling design. *Limnol. Oceanogr.* **66**: 4063–4076. doi:[10.1002/lno.11943](https://doi.org/10.1002/lno.11943)
- Rudberg, D., and others. 2021. Diel variability of CO₂ emissions from Northern Lakes. *J. Geophys. Res.: Biogeosci.* **126**: e2021JG006246. doi:[10.1029/2021JG006246](https://doi.org/10.1029/2021JG006246)
- Sieczko, A. K., N. Thanh Duc, J. Schenk, G. Pajala, D. Rudberg, H. O. Sawakuchi, and D. Bastviken. 2020. Diel variability of methane emissions from lakes. *Proc. Natl. Acad. Sci. USA* **117**: 21488–21494. doi:[10.1073/pnas.2006024117](https://doi.org/10.1073/pnas.2006024117)
- Vachon, D., and Y. T. Prairie. 2013. The ecosystem size and shape dependence of gas transfer velocity versus wind speed relationships in lakes. *Can. J. Fish. Aquat. Sci.* **70**: 1757–1764. doi:[10.1139/cjfas-2013-0241](https://doi.org/10.1139/cjfas-2013-0241)
- van Bergen, T. J. H. M., and others. 2019. Seasonal and diel variation in greenhouse gas emissions from an urban pond and its major drivers. *Limnol. Oceanogr.* **64**: 2129–2139. doi:[10.1002/lno.11173](https://doi.org/10.1002/lno.11173)
- Varadharajan, C., and H. F. Hemond. 2012. Time-series analysis of high-resolution ebullition fluxes from a stratified, freshwater lake. *J. Geophys. Res.: Biogeosci.* **117**: G02004. doi:[10.1029/2011JG001866](https://doi.org/10.1029/2011JG001866)
- Waldo, S., J. J. Beaulieu, W. Barnett, D. A. Balz, M. J. Vanni, T. Williamson, and J. T. Walker. 2021. Temporal trends in methane emissions from a small eutrophic reservoir: The key role of a spring burst. *Biogeosciences* **18**: 5291–5311. doi:[10.5194/bg-18-5291-2021](https://doi.org/10.5194/bg-18-5291-2021)
- Walsby, A. E. 1997. Numerical integration of phytoplankton photosynthesis through time and depth in a water column. *New Phytol.* **136**: 189–209. doi:[10.1046/j.1469-8137.1997.00736.x](https://doi.org/10.1046/j.1469-8137.1997.00736.x)
- Wang, X., and others. 2017. Greenhouse gases concentrations and fluxes from subtropical small reservoirs in relation with watershed urbanization. *Atmos. Environ.* **154**: 225–235. doi:[10.1016/j.atmosenv.2017.01.047](https://doi.org/10.1016/j.atmosenv.2017.01.047)
- Webb, J. R., P. R. Leavitt, G. L. Simpson, H. M. Baulch, H. A. Haig, K. R. Hodder, and K. Finlay. 2019. Regulation of carbon dioxide and methane in small agricultural reservoirs: Optimizing potential for greenhouse gas uptake. *Biogeosciences* **16**: 4211–4227. doi:[10.5194/bg-16-4211-2019](https://doi.org/10.5194/bg-16-4211-2019)
- Wetzel, R. G. 2001. Land-water interfaces: Larger plants, p. 528–577. *In* *Limnology*. Academic Press.
- Whiting, G. J., and J. P. Chanton. 1996. Control of the diurnal pattern of methane emission from emergent aquatic macrophytes by gas transport mechanisms. *Aquat. Bot.* **54**: 237–253. doi:[10.1016/0304-3770\(96\)01048-0](https://doi.org/10.1016/0304-3770(96)01048-0)
- Wickham, H. 2016. *ggplot2: Elegant graphics for data analysis*. Springer.
- Zhao, J., and others. 2019. An evaluation of the flux-gradient and the eddy covariance method to measure CH₄, CO₂, and H₂O fluxes from small ponds. *Agric. For. Meteorol.* **275**: 255–264. doi:[10.1016/j.agrformet.2019.05.032](https://doi.org/10.1016/j.agrformet.2019.05.032)

Acknowledgments

We thank members of the Rosemond, Wenger, and Freeman labs for their sampling assistance, especially Emily Chalfin, Olivia Allen, Ally Whit-eis, John Knox, Justin Weimorts, Lee Dieterich, and Mackenzi Hallmark. We thank John Pickering for access to Blue Herron, where blue herons are sometimes observed. We also thank two anonymous reviewers for providing comments which improved the manuscript. This research was conducted as part of the Network for Engineering with Nature (N-EWN; <https://n-ewn.org>). This work was supported by the U.S. Army Corps of Engineers Engineering With Nature® Initiative through Cooperative Ecosystem Studies Unit Agreement W912HZ-20-20031. The use of products or trade names does not represent an endorsement by either the authors or the N-EWN. Opinions expressed here are those of the authors and not necessarily those of the agencies they represent or the N-EWN.

Conflict of Interest

None declared.

Submitted 05 October 2023

Revised 26 January 2024

Accepted 05 April 2024

Associate editor: John Downing